Flexible conductive substrate incorporating a submicron co-continuous polyaniline phase within polyethylene by controlled crazing

Anton B. Kornberg,[a] *Michael R. Thompson,*[b] *Shiping Zhu* [ab]*

[a] Department of Chemical Engineering, McMaster University, Hamilton, Ontario, Canada

[b] School of Science and Engineering, The Chinese University of Hong Kong, Shenzhen, Guangdong, China 518172.

* Author to whom correspondence should be sent. E-mail: shipingzhu@mcmaster.ca

Keywords: electrical conductivity, polyethylene, polyaniline, emulsion, co-continuous structure, crazing, flexible electronics.

ABSTRACT

A polyethylene film with an incorporated nano-dispersed polyaniline conductive network was developed by controlled crazing in a high-pressure reactor while immersed in an emulsified medium of aniline in chloroform. The resulting conductive material exhibited an average through-plane electron conductivity of 2×10^{-2} S·cm^{-1}, within an order of magnitude of brittle doped polyaniline (1.2×10^{-1} S·cm^{-1}) yet retained the ductility of the polyethylene matrix. It was

also shown that 90% of the original conductivity was retained after 18% (about 0.9 mm) elongation. Embedded polyaniline fibers acted both as a nucleating agent to reduce the size of crystallites for controlled crazing and as submicron conductive nodes, connecting neighboring conductive conduits formed inside the crazing voids, with both effects contributing to the increasing electrical permeability of the secondary phase. For comparison, montmorillonite and TiO_2 particles were tested as alternative nucleating agents to verify the effect of the preliminary embedded polyaniline fibers on the matrix morphology and, consequently, the conductivity acquired.

1. INTRODUCTION

Among the familiar group of intrinsically conductive polymers, polyaniline (PANI) has become a focal point of interest due to its combination of properties such as stability in aggressive chemical environments, extremely low solubility in water and most known solvents, thermal stability, and non-toxicity. The mechanism of synthesis and oxidizing (doping) of PANI is well-studied,[1–3] with its high conductivity notably reversible by adjusting its surrounding pH.[4] Such characteristics have made doped PANI highly attractive as a material for adjustable sensing of acids,[5,6] alcalis,[7] and various organic substances,[8,9] via monitoring the electrical conductivity of PANI while it is in contact with the investigated chemicals.

However, PANI has a variety of disadvantages such as a tendency to decompose at ~200 °C,[10] below its melting temperature, and its known brittleness and low strength,[11] which greatly limit its utility and reliability as a material for flexible sensors fabrication. One of the ways to balance this mechanical weakness and expand the scope of application of PANI is to embed it into a mechanically durable and elastic matrix but there are significant challenges with

establishing a percolating secondary phase for conductivity without high loadings such that the flexible nature of the matrix is not lost.

The conventional method for imparting conductivity to non-conductive matrices by admixing them with conductive solid fillers is not always an adequate long-term solution; PANI has such a high melting temperature it is usually considered a solid filler in most compounded polymer systems. The dispersed particles form permeable structures in the matrix volume only at relatively high content, which produce very high processing viscosities during their preparation and present solid-state property sensitive to deformation. Ideally, co-continuity of a conductive secondary phase at relatively low content is envisioned as a more desirable material system. Such an alternative approach could consist of polymerizing conductive liquid reactants within the cavitated space of a matrix to form nano-to-micron scaled channels in an otherwise ductile material. The mixture of reactants serves an added role in the method, foreseeably acting as a surface-active liquid medium to facilitate controlled cavitation along the crystallite boundaries during matrix plastic deformation.

The described alternative approach above is based on the mechanism of crazing in polymers in the presence of liquids, similar to the damaging phenomenon that occurs naturally during part service via Environmental Stress Cracking (ESC).[12,13] In our previous research,[14] we extended the approach of Volynskii et al.,[15,16] and Rozanski et al.[17] to control polymer crazing in liquid surroundings for our purposes of developing a percolating secondary phase as a functional network within a polyethylene matrix. To increase the efficiency of the method, TiO_2 nucleating particles can be added into the matrix polymer, thereby reducing the crystallite size and expanding the crystal-amorphous interfacial area, which, in turn, caused a rise in the number of primary voids[18,19] followed by growth in the density of crazes.[20,21] The resulting material

possessed nano-scaled channels that percolate through the matrix, consisting of the secondary phase at low volume fraction. Since thin or narrow structures tend to be more prone to displaying a flexible nature compared to bulk materials, it is hypothesized that this approach may be suitable for creating flexible electronic components, something very attractive in the field of wearable technology.

Therefore, the present research aims to further advance the approach investigated earlier for the purpose of now producing a highly conductive yet ductile polymer alloy featuring a percolating network of PANI within a polyethylene matrix. Different nucleating agents were investigated to determine their persistent role on the resulting conductivity properties of the material after their initial function of controlling the crystallinity of the matrix.

2. EXPERIMENTAL METHODS

2.1. MATERIALS

Linear low-density polyethylene (LLDPE LL 8460.29, ExxonMobil Chemical), titanium dioxide nanoparticles (TiO_2 P25 AEROXIDE, Degussa), and montmorillonite particles (Cloisite 30B, Southern Clay Products) were used as received. The TiO_2 had a quoted particle size of 21 nm by the supplier. Fractions of the montmorillonite with a particle size of less than or equal to 2, 6, and 13 μm were of 10, 50, and 90%, respectively. Aniline (≥99.5%, Aldrich), 4-dodecylbenzenesulfonic acid (DBSA) (DBSA, mixture of isomers ≥95%, Aldrich), Ammonium persulfate (APS, ≥98%, Aldrich), Lithium chloride (LiCl, ≥99%, Aldrich), Xylene (≥98.5%, mixture of the isomers, Aldrich), and Chloroform (≥99%, Aldrich) were used as received.

2.2. PREPARATION OF PANI FIBERS

Traditionally, aniline is polymerized in an aqueous solution. In this research, polymerization of both the pre-synthesized polyaniline fibers and the subsequently introduced secondary polyaniline phase in polyethylene, were carried out in the weakly polar solvents of xylene and chloroform, respectively. The monomer and surface-active agent (DBSA) formed an anilinium-DBSA complex, as shown in Fig. 1, which presented itself as micelles[22] in the solvents; the DBSA hydrophobic tails were directed outward to the highly compatible solvent molecules and subsequently, to the matrix polyethylene.

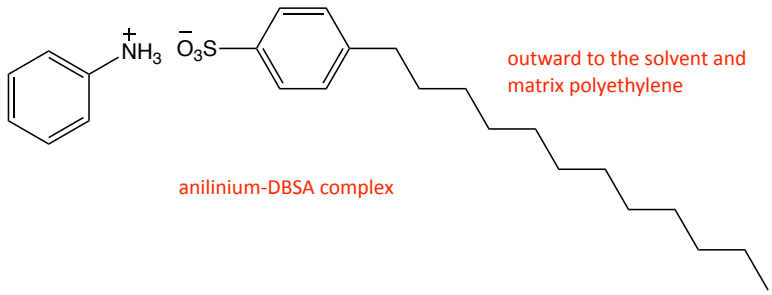

Figure 1. Structure of intermediate anilinium-DBSA complex as a preliminary step in the polymerization of PANI for fibers.

The recipe for pre-synthesized polyaniline fibers as a nucleating agent in the polyethylene was mainly adopted from the research by Osterholm et al.[2] A solution of 4.65 ml of aniline and 24.48 g of DBSA in xylene (Aldrich) was cooled down to 0 °C. Polymerization was initiated by the addition of 4.68 g of APS into 20 ml distilled water, introduced dropwise over 30 min under vigorous agitation, as the reaction is quite exothermic. The total polymerization time was 24 hrs. After synthesis, the precipitate was centrifuged and stored for further use.

Some portion of the precipitate was washed and dried as a film to measure the conductivity of the pure material, which was found to be $1.2\times10^{-1} \pm 3.5\times10^{-2}$ S·cm^{-1}. The color of the precipitate was dark green, which corresponds to the emeraldine salt form, with a slight blue tint that indicates the partial inclusion of the deprotonated emeraldine base form.[23]

2.3. PREPARATION OF MATRIX SAMPLES

Fabricating the films of LLDPE, powder was dissolved in xylene at 132 °C and then premixed with one of three types of nucleating agents: pre-synthesized PANI-DBSA fibers in the amount of 5% (w/w) to pure LLDPE (denoted as P); Cloisite 30B particles in the amount of 5% (w/w) to pure LLDPE (denoted as C); or TiO_2 nanoparticles in the amount of 2% (w/w) to pure LLDPE (denoted as T). The solution was cast on aluminum substrates and then kept in an oven at 80 °C under vacuum overnight to remove xylene residues.

The final cast film had a thickness of 110±10 μm. Dumbbell-shaped samples were cut out of the film with a middle-narrowed section being 5 mm long and 5 mm wide, and larger ends for mounting in the tensile rig mentioned below.

2.4. DEFORMATION OF SAMPLES AND POLYMERIZATION

The deformation procedure was basically adopted from the previous research.[14] The tensile rig with the mounted sample, while immersed in the prepared emulsion, was placed inside a high-pressure reactor with a maintained temperature controlled by a circulating refrigerant fluid. The tensile strain was applied to the samples step-wise at 0.25 mm per cycle increments, so as to maintain the resulting rate of deformation constant at 0.03 mm·min^{-1}. A pressure of 2.76 MPa was created inside the reactor with high purity nitrogen gas after preliminary purging. The

deformation was performed until the degree of longitudinal elongation of the middle-narrowed section reached 25, 50, 75 or 100% strain. The percent elongation was used following the capital letters, P, C, and T, in the naming convention of completed samples. For example, the sample denoted as T50 contained TiO_2 nucleating particles and its middle-narrowed section increased in length by 2.5 mm, up to 7.5 mm in total.

The emulsion, within which the samples were deformed, was prepared as follows. Under vigorous agitation, 0.285 g of aniline was added dropwise to a solution containing 1.53 g of DBSA in chloroform, after which the total volume of the emulsion was brought up to 16 ml with chloroform. After emulsion homogeneity was achieved, its temperature was decreased to –17 °C. 0.3 g of APS was dissolved in 1.25 ml of distilled water, with the addition of 2.623 g of LiCl to keep the solution unfrozen. The solution was cooled down to –17 °C and then added dropwise to the emulsion under vigorous agitation.

Chloroform, as a weakly polar solvent, has proven to be an effective penetrating liquid; its surface energy is of 0.0299 $N \cdot m^{-1}$,[24] which is fairly close to that of polyethylene, 0.0353 $N \cdot m^{-1}$.[25] This was in agreement with the research by Rozanski et al.[26] who suppressed gross failure in polymers by exposing them to chloroform while undergoing deformation. Chloroform was also used due to the ease of its removal from the final composites, as compared to xylene. The lower emulsion viscosity was also an advantage giving the solution a higher penetration capacity, as well as the facilitated agitation of the reaction mixture while the sample is saturated at deformation, as well as while the mixture is polymerized, especially in the later stages, when its viscosity increased.

The low reaction temperature was due to the need to inhibit the decay of APS and thus ensure that the cavitated matrix was fully impregnated with the reaction mixture before

polymerization began. After the sample deformation was completed, the temperature of the reaction cell was elevated up to 0 °C and maintained at this condition for 24 hrs, enabling APS to decay and initiate polymerization directly in the cavitated space of the matrix.

2.5. ELECTRICAL CONDUCTIVITY MEASUREMENT

After vacuum drying at 80 °C for 24 hrs, elongated dumbbell samples were polished by sandpaper on both sides to remove any polyaniline-deposited film on their surfaces. The edges of the samples, possibly more enriched by polyaniline, were also cropped to avoid electrical current circumventing a path through the sample.

The probes, both with faces of the same contact area A, were formed by depositing a conductive nickel paste on both surfaces of the obtained specimens. Silver-plated wires were embedded into the probes and connected to an Agilent 34401A 6½ Digit Multimeter. Direct current (DC) resistivity was calculated as $\varrho = (R \cdot A)/L$, where R was the measured resistance. The specimen thickness, which is equivalent to the distance between the probes, was taken as dimension L in the resistivity calculation. The DC conductivity σ [$S \cdot cm^{-1}$] was then calculated by the formula $\sigma = 1/\varrho$. To maintain consistency, the resistance was always taken ten seconds after the closure of the measurement loop.

2.6. MECHANICAL CHARACTERIZATION

A benchtop Model 3366 Universal Mechanical Testing System (Instron Corporation; Canton, MA) was used for the strain-controlled tensile tests and stretchable conductivity response measurements. The system was equipped with a 500 N load cell and operated at ambient room temperature. For each sample, thickness was measured with a digital caliper at

three points in the narrowed section. Testing was performed at a strain rate of 2.5 mm·min^{-1} until failure. At least three repeated measurements were performed for each test.

2.7. STRETCHABLE CONDUCTIVITY RESPONSE

The flexibility of the PANI secondary phase within samples was evaluated for both through-plane and in-plane conductivity, as schematically shown in Fig. 2a and Fig. 2b, respectively, by measuring resistance R while simultaneous stretching the samples in the same mechanical testing system, at a strain rate of 2.5 mm·min^{-1}, until the conductivity dropped below the limit of the measurement device.

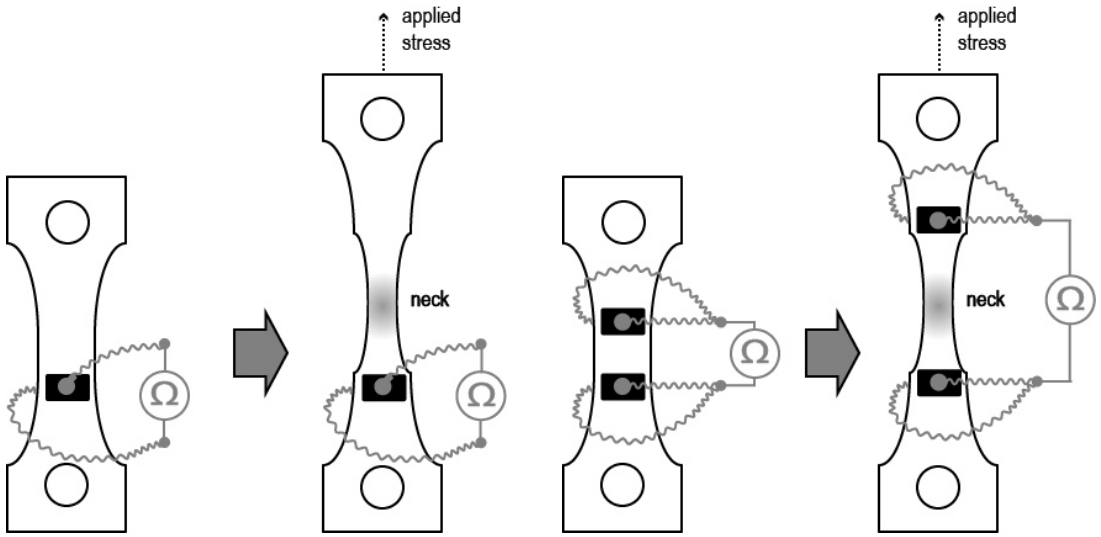

Figure 2. Specimens for (a) through-plane and (b) in-plane conductivity measurements.

For through-plane conductivity, the measurement was carried out through a couple of contralateral probes mounted on opposite sides of the specimen. For in-plane conductivity, the measurement used a second set of probes mounted at an initial distance of L, which then

increased with stretching. Dimension *A* for the resistivity was equal to the product of the probe width (the length of the probe edge perpendicular to the specimen) and the thickness of the specimen, before stretching. Since the dimension *A* cannot be assumed to be fixed during stretching of the specimen, the reported values cannot be considered an accurate value of conductivity, but served well to demonstrate the persistence of electron pathways as the PANI channels were distressed.

The results revealed an inflection point on the through-plane conductivity curve corresponding to a specimen elongation of ~1% strain, until which conductivity remained almost unchanged. In this range, deformation was close to elastic, as indicated by the nearly linear behavior of the stress-strain curve. Based on this, the specimens were subjected to cyclic loading, at the same strain rate of 2.5 $mm \cdot min^{-1}$, with subsequent relaxation, for 20 cycles in total, with simultaneous measurement of through-plane conductivity.

2.8. MORPHOLOGICAL CHARACTERISATION

A JEOL JSM 7000 scanning electron microscope (SEM) was used to obtain micrographs for morphology analysis. A sample was cryogenically fractured in its narrowed section and the exposed cross-section was sputter-coated with a 5 nm thick layer of platinum. To determine the individual pore sizes and secondary phase distribution, images were processed using ImageJ software (National Institute of Health, U.S.). The processing results were based on five hundred occurrences of pores in each image.

A Zeiss Axioplan 2 light microscope was used to characterize the pre-synthesized PANI fibers dispersed in xylene, and evaluate the effect of the different nucleating agents on the crystallinity of the matrix. To prepare a specimen of the fibers, a drop of non-centrifuged

suspension was placed on a slide, under a coverslip and immediately examined. Specimens of the matrix were prepared by placing a drop of heated (132 °C) solution of polyethylene with a corresponding nucleating agent, was placed on a slide, under a coverslip, and then kept at 80 °C overnight under vacuum before examination.

3. RESULTS AND DISCUSSION

3.1. PRE-SYNTHESIZED PANI FIBERS

The emulsion polymerization method produced a threadlike structure of PANI in suspension. This fibrous form was similarly reported by other researchers using this polymerization method.[11,27] The aligned chain arrangement of PANI result in high electrical conductivity due to a low impedance to interchain charge diffusion along the final fiber [28,29]. The emeraldine colored PANI fibers in xylene, prepared by the technique described in section 2.8, are shown in Fig. 3. The image shows comparable fractions of both short (2-3 μm) and long (up to 10 μm) fibers were present in the suspension, which can be attributed to uneven distribution of DBSA during the synthesis.[30,31] Long hydrophobic tails of DBSA stabilize and orient the PANI chains with the formation of a fiber. Accordingly, a low concentration of DBSA yields the short fiber regions in the image, which are characterized by a blue tint due to insufficient protonated polyaniline emeraldine base.

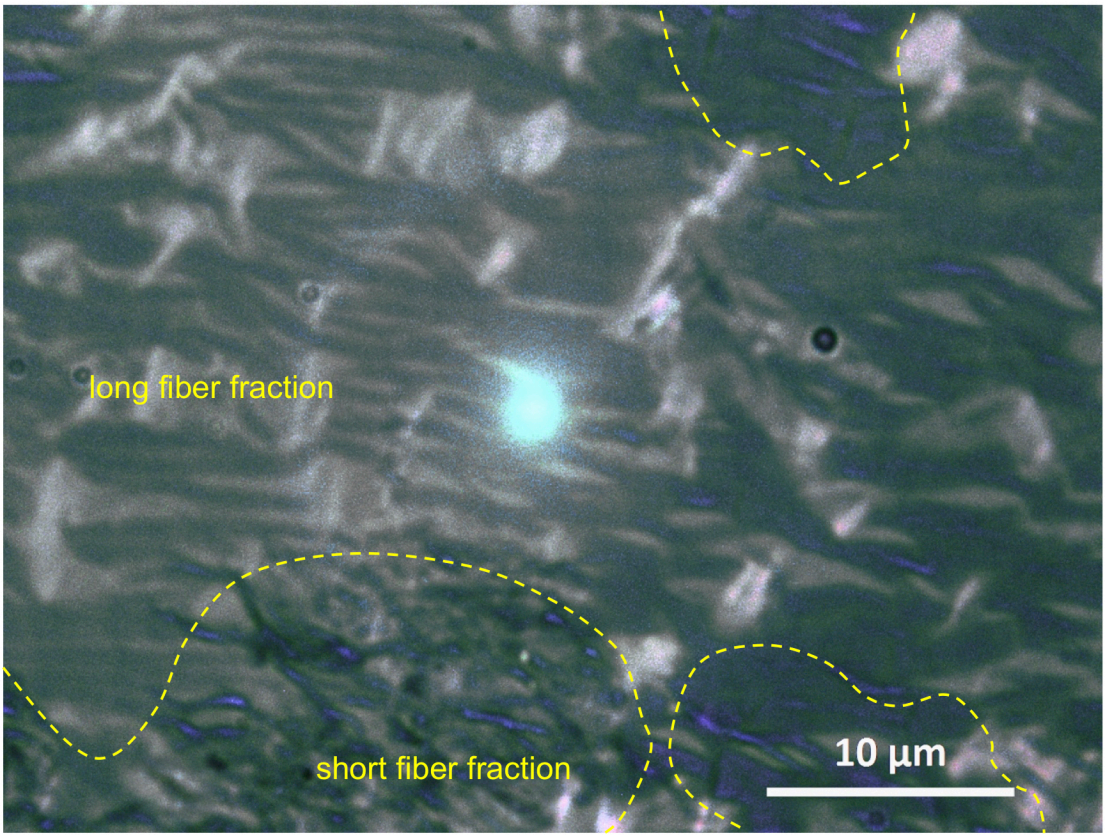

Figure 3. Pre-synthesized PANI fibers in xylene with two distinguishable lengths of fiber present. Dashed lines indicate the boundaries of clusters with fibers of different lengths.

When choosing the initial nucleating agent content for the fibers, a balance between conductivity of the final samples and their mechanical characteristics was considered. With an increase in the content of fibers, the yielding behavior of the matrix showed much more fragmentary plastic damage. Microscopic analysis showed visible agglomerations of polyaniline fibers between crystallites at higher than 5 wt% content, which apparently led to the mechanical instability of the matrices. Conversely, at a lower percentage of fibers, a noticeable drop in conductivity of the final samples was observed, probably due to an insufficiently developed

distribution of junctions for the subsequent polyaniline network, which could not effectively contribute to the percolation requirements of the secondary polyaniline phase.

3.2 EFFECT OF NUCLEATING PARTICLES ON MATRIX MORPHOLOGY

All three nucleating agents showed good dispersion in the polyethylene solution with xylene. Few aggregates were seen in the solution itself or in the cast films. The organic coating of Cloisite 30B was beneficial in this regard. Similarly, for the PANI fibers, the embedded DBSA with its protruding alkyl tails from the surfaces of the fibers ensured their compatibility with the polyethylene matrix, improving the van der Waals interactions.

The size of the polyethylene crystallites was shown in a previous study to be reduced by the addition of TiO_2 nucleating nanoparticles, which results in an increased crystal-amorphous interfacial area.[14] Crystallites of approximately 1 μm or less in size, are shown in the optical micrograph in Fig. 4a with TiO_2 as a nucleating agent. For comparison, pure polyethylene displayed larger crystallites of about 100 μm (Fig. 4b). Montmorillonite and PANI fibers were tested as alternative nucleating agents, and both found to yield similar average sized polyethylene crystallites of about 5 μm, shown by optical micrographs in Fig. 4c and 4d, respectively. The crystallite sizes found in sample type C with montmorillonite were, however, more homogeneous while sample type P had distinct regions of larger and smaller crystallites (separated by a yellow dotted line). The variation in crystallite size was attributed to the presence of two size fractions of polyaniline fibers, which is explained in the next section. The micrograph for sample type P shows the green polyaniline fibers are displaced along the inter-crystalline boundaries. The fibers are not well connected by the alignment along the boundaries was enough to result in a low, but detectable conductivity of undeformed matrices, equal to about 6×10^{-9} $S\cdot cm^{-1}$. Neither the pure

polyethylene or samples type C and T showed any detectable conductivity within the sensitivity of the multimeter.

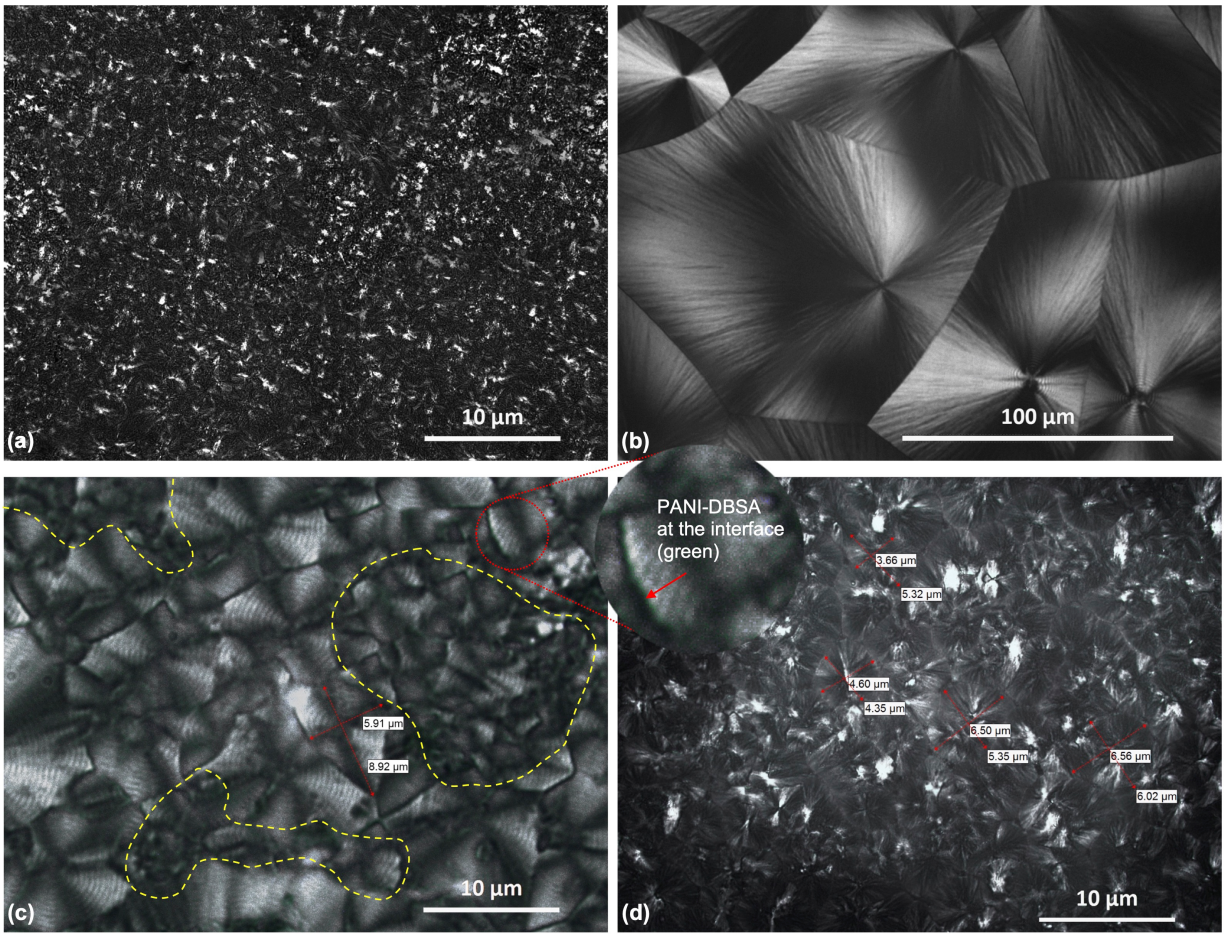

Figure 4. Morphology of LLDPE matrices with (a) LLDPE matrix with TiO_2 (image was taken from the previous paper[14]) and (b) pure LLDPE matrix, compared to (c) PANI fibers [type P] or (d) Cloisite 30B [type C] nucleating agents. Magnification differences due to the scale of morphological detail to be shown.

3.3. RESULTING MORPHOLOGY AND MASS CHANGE

The morphology of P100, C100 and T100 were examined by SEM and respectively shown in Fig. 5a, 5b, and 5c. The micrographs highlight a randomly selected region from the fractured surface, at a distance of approximately 10 μm from one of the specimens' edges.

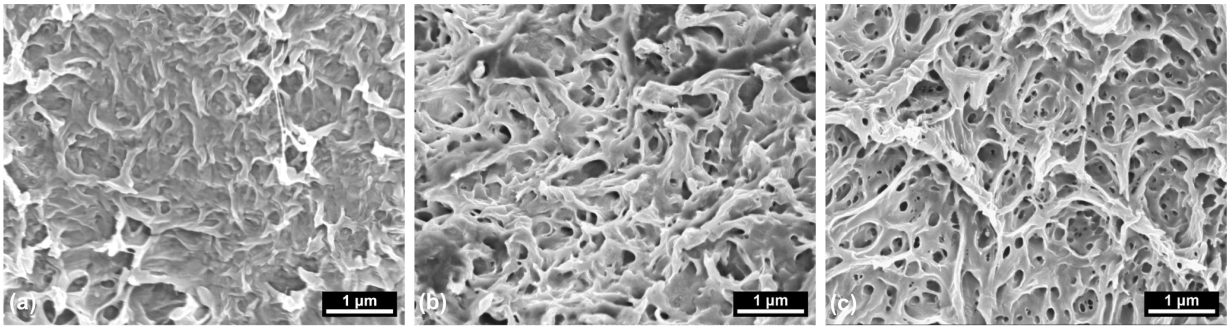

Figure 5. SEM morphology of samples (a) P100, (b) C100 and (c) T100 exposed by cryogenically fractured normal to the deformation axis. A varying degree of porosity was evident as the PANI secondary phase filled in the cavitated network formed by stretching polyethylene in aniline-DBSA emulsion in chloroform.

A network of PANI had effectively filled the cavitated structure of the polyethylene in the case of P100. The smooth dark regions seen in the SEM image for P100 were believed to correspond to the brittle polyaniline phase, while the white rough regions were considered to be fibril protrusions corresponding to the ductile polyethylene phase; PANI is a brittle polymer and the least likely of the two polymers to fail via fibrillation during cryofracturing. Based on image analysis of these micrographs, the cross-section for P100 showed the least porosity, estimated at 5% based on the displayed surface area. For C100, the total porous area found was 11%, while

for T100 it was 35%, with hierarchical porosity and a pore area variation being in the order of 0.001-0.1 μm^2. The characteristics of porosity for each sample type are summarized in Table 1.

Table 1. The results of the SEM micrographs' image analysis for P100, C100, and T100.

	Total unfilled area, %	Total number of pores
P100	5	18
C100	9	129
T100	35	308

There were considerable concerns for the pore size in this study, controlling the mass fraction of the secondary phase as well as influencing the conductivity and flexibility of the final material. In regards to mass gain, the physical size of the micelles formed by the anilinium-DBSA complex would limit their entry into the strain-developed crazes until the pore was large enough, making the pores a significant factor in the extent of PANI-filled regions seen in the micrographs. The micelle size and structure can vary significantly depending on the ratio of aniline to surfactant. Several other research groups conducted the synthesis under similar conditions, and reported that the micelles can be up to 250 nm in size,[32] but can also form agglomerates up to ~1 μm in diameter.[22] In order to estimate the approximate size of emerging crazes, the crystal fraction should be considered unaffected while the polymer matrix is stretched in a thermodynamically compatible liquid medium, as established by Rozanski et al.[26] and later by our previous research.[14] The matrix is elongated only due to uniform cavitation of its amorphous fraction, as a result of which, the finer crystal structure of the matrix results in the smaller diameter of the emerging crazes, for equal elongations.

Accordingly, the cavitated structure of matrices P and C with their average initial crystallite size of 5 μm (Fig. 4) crazed yielding pore sizes better to accommodate the emulsion micelles than matrix T with an average crystallite size of 1 μm and less. Low molecular weight chloroform, being highly compatible with polyethylene, freely penetrated all types of matrices and decreased the mechanical energy threshold for craze initiation,[20] regardless of the total amount of absorbed emulsion. This was evident for T100, shown in Fig. 5c, with a visible absence of dark areas associated with the secondary polyaniline phase but still showing a high number of evenly distributed small cavities.

Fig. 6 shows changes in mass of the three sample types prepared in the study, at different degrees of elongation. The case in which an effectively cavitated sample showed insignificant mass increase corresponding to the introduced secondary phase of PANI is shown by sample type T; preliminary tensile testing of the matrix has shown that any strain greater than 1% will result in plastic deformation and hence all tested states in this figure correspond to permanent damage. A noticeable improvement in mass gain was only seen upon reaching an elongation of 75% (denoted as A in the figure) for type T, indicating an adequate change in the diameter of crazes for which penetration of the emulsion into the matrix increased. The lower PANI phase content of this sample type noted by this mass gain was similarly attributed to the very ductile nature of the final sample in Fig 5, noted by the substantial fibrillation in the micrograph. Furthermore, shrinkage was notably higher for T100 than seen for P100 once the sample was removed from the reactor, which again confirmed our conclusion that sample type T included less of the PANI secondary phase. Interestingly, the shrinkage for T100 specimens was similar to C100, which would not be expected from the mass gain data. We believe this can be attributed

to the enriched PANI outer layers seen for T100, adding rigidity and hence resistance to shrinkage until it was eventually removed by sanding.

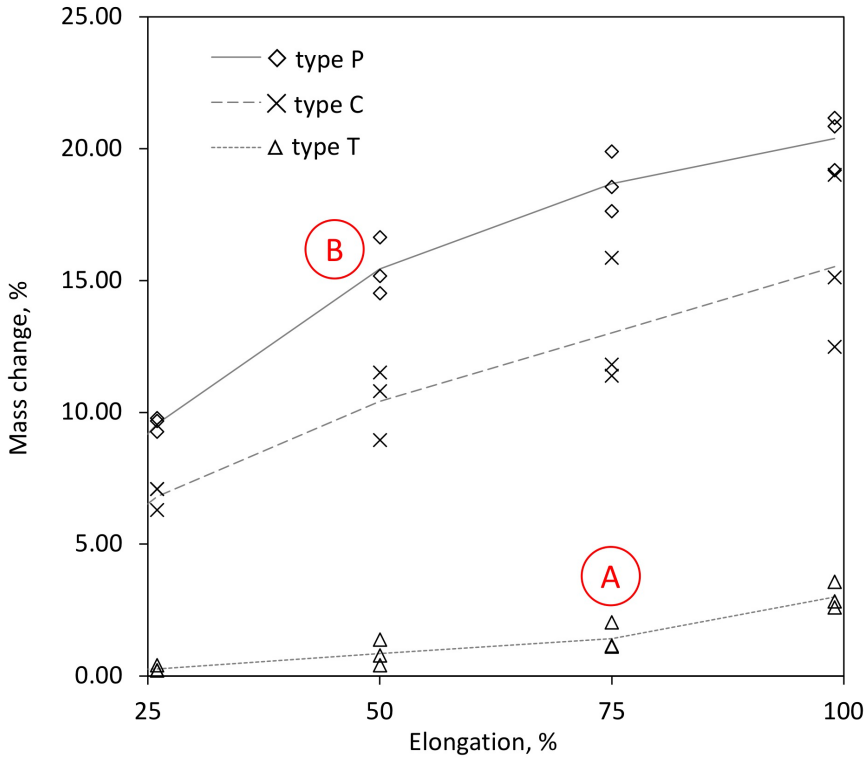

Figure 6. The effect of different degrees of elongation on the sample mass change due to formation of the secondary phase of PANI. The lines are included to visually highlight average tendency.

Samples of type P and C showed substantial mass gain in Fig. 6, with type P showing the greatest mass gains of all three types prepared in the study. Mass changed rapidly up to 10wt% for type P by an elongation of 25%, and then up to 15wt% at 50% elongation (denoted as B on the graph). As discussed above, the larger diameter of crazes for this sample type led to a higher

absorption rate of the anilinium-DBSA emulsion, even at a low extent of deformation. The fibers initially embedded in the matrix additionally promoted the movement of the emulsion micelles through crazes due to high thermodynamic compatibility, as discussed below. The rate of further mass gain decreased slightly and reached 20wt% for P100. Taking into account the mass of the fibers initially embedded into the matrix, the amount of PANI-DBSA secondary phase in the completed blends yielded 25wt%. Samples of type C showed less mass gain in the graph and underwent more noticeable shrinkage after removal from the reactor, compared with samples of type P. The shrinkage mentioned is attributed to stress relaxation upon removal from the reactor and no longer being subject to fixed strain, with the dimensional change being greater when less polyaniline was present to fill the voids created by cavitation. Compared with samples P, the mass gains for samples of type C were lower, reaching only to 15wt% for C100. Given the same average crystallite size for samples P and C (Fig. 4a and 4b), we can expect an equal diameter of the opening crazes, and therefore a similar pattern of matrix saturation by the emulsion droplets, The obtained difference is explained by lower compatibility of the emulsion micelles with the matrix material containing embedded montmorillonite particles rather than embedded PANI fibers. The high degree of fibrillation on the surface of C100 in Fig. 5 had a quite significant ductile fraction, but at the same time exhibited a fairly low porosity.

The size of matrix crystallites (influenced by the nucleating agent) and penetrating liquid collectively influenced the intensified formation of a crazed network. A higher frequency of crazes decreased the potential for increased pore sizes at the same degree of sample elongation, which in turn mitigated the loss of the matrix mechanical properties. It was determined, however, that an excessively developed network forms crazes with a diameter insufficient for the passage of the emulsion micelles, resulting in poor absorption of the secondary phase material by the

matrix. The use of PANI fibers as nucleating particles provided the optimal crystallite size, as well as ensured better affinity of the matrix cavitated interior to the emulsion micelles, which, in turn, resulted in the highest mass increase at equal degrees of sample elongation, with the formation of the visually homogeneous composite.

3.4. ELASTIC MODULUS CHANGE

Fig. 7 shows the Young's modulus of samples of types P, C, and T, produced at differing degrees of elongation after being immersed in the emulsion. Samples of type T showed higher elastic moduli for all levels of elongation compared to the other types, due to its finer crystallite structure and reinforcement by TiO_2. The undeformed samples of type C showed a larger modulus than type P, due to the higher mechanical strength of montmorillonite particles and their correspondingly better reinforcement of the LLDPE matrix than PANI fibers.

While matrices were deformed, uniform cavitation occurred due to the penetration of chloroform, which resulted in a decline in modulus for all samples. At 100% elongation, the modulus of samples had decreased by 53%, 70%, and 52% corresponding to sample type P, C, and T respectively. Cavitation had a much more significant effect on mechanical properties for samples of type C, with a drop in modulus by 47% at only 25% strain. For the same strain and average crystallite size of type P, its modulus decreased by only 32% due to comparatively improved bonding with its filler as a result of the hydrophobic tails of DBSA molecules. The more moderate decrease in modulus for P compared with C may also be related to the reinforcing nature of a fiber versus a particle, resulting in more effective stress transmission. Compared with C and P, type T demonstrated the more moderate decrease in modulus at 25% strain. This was due to the finer crystallites, which appears to be more stable during matrix deformation than the reinforcing effect of embedded particles.

At deformations higher than 50% strain, all three types show a decline in the rate of strength loss. Type P demonstrates a smaller rate of loss at higher strain due to the continuous polyaniline phase connecting the originally added fibers to add rigidity to the sample. The onset of this described plateau began at lower strain compared to the other sample types due to this continuous secondary phase (as demonstrated by the results for through-plane conductivity, next section).

Type C samples, according to the mass change results, acquired a certain amount of PANI, but this secondary phase did not form many continuous channels (as evident by its low conductivity) to add reinforcement to the matrix. Subsurface material accumulation was possible, which ensured some reinforcement at high deformations, but at the same time, resulted in considerable scatter in the results. For type T, the PANI phase did not appear to penetrate the matrix in any significant quantities, which is consistent with the results for mass change and conductivity.

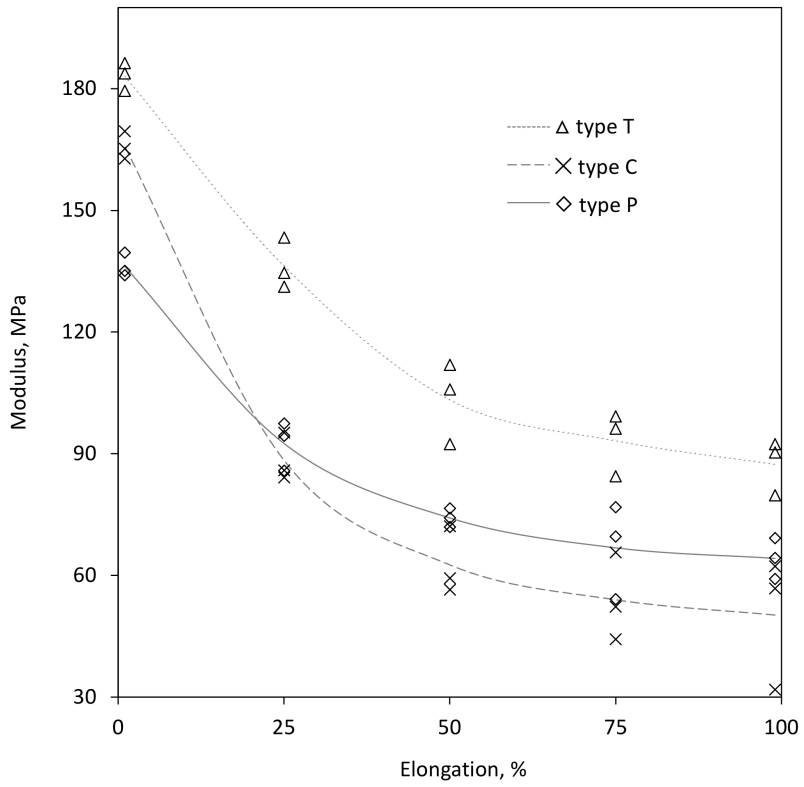

Figure 7. Effect of the elongation and particle type on Young's modulus of the material.

3.5. THROUGH-PLANE CONDUCTIVITY

Electrical conductivity is a relatively simple and reliable way to determine continuity of the secondary phase within the polyethylene matrix. The bulk through-plane measurement was calculated based on the apparent volume of the tested samples, without taking into account the morphology of the conducting phase, as DC conductivity depends only on the total secondary phase cross-section and does not depend on the diameter of its individual channels. The conductivity of the three sample types is shown in Fig. 8 based on the extent of elongation during their preparation. Samples of type T demonstrated negligible conductivity relative to the

sensitivity of the multimeter until the elongation was 75%. This matches the measured mass gains in the previous sections where it was concluded that the emulsion micelles had difficulty passing into the crazes until the pores were large enough, and so could not effectively be deposited with the formation of the conductive secondary phase. From 75% to 100% elongation (denoted as A in the graph), there was a subtle increase in conductivity, up to 10^{-8} S·cm^{-1}. The low mass gain and low conductivity together suggest that the formed percolative network was poorly developed, though interference by the TiO_2 was a possible contributing factor.

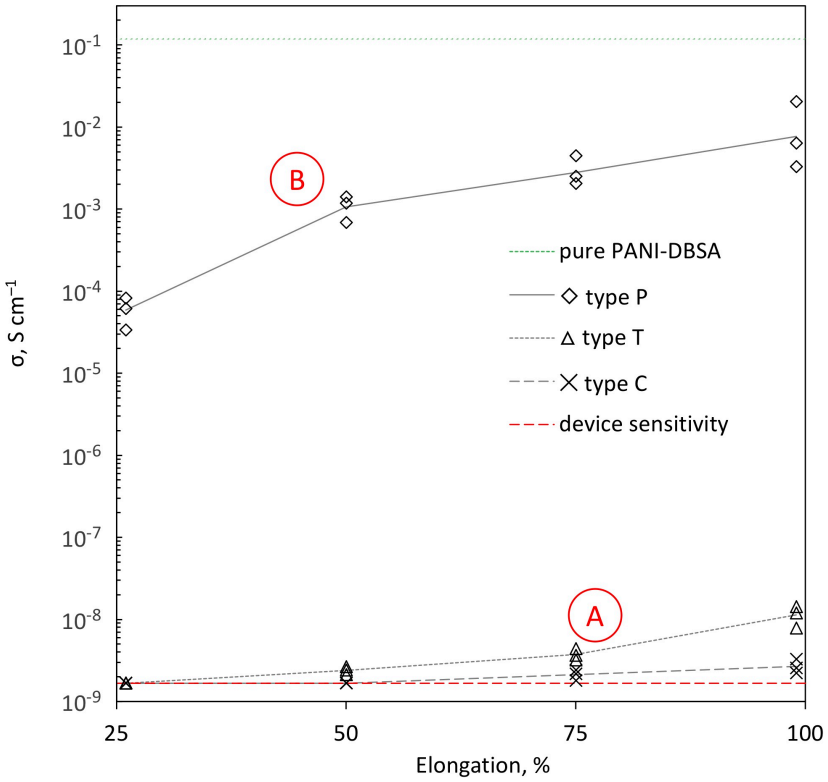

Figure 8. Through-plane conductivity of the samples with the different types of particles as a function of elongation.

Samples of type P and C had similar crystallite sizes and hence would have been expected to craze similarly. Both sample types showed significant mass gains to indicate adequate deposition of the conductive secondary phase in the cavitated matrix of polyethylene as a result of elongation. It was therefore interesting how different in conductivity these two sample types were in testing. At 50% elongation, the measured average conductivity for P50 (denoted as B in the graph) was 1.06×10^{-3} S·cm^{-1}, whereas it was only 1.67×10^{-9} S·cm^{-1} for C50. At 100% elongation, P100 showed an average conductivity of 2×10^{-2} S·cm^{-1}, which was close enough to a conductivity of the reference sample of pure PANI-DBSA, 1.2×10^{-1} S·cm^{-1}. Conversely, the conductivity for C100 conductivity showed no significant change compared with C50. The two curves representing the results for type C and P appear to be demonstrating the effects of embedded nucleating agent as junctions in conductive network since the mass gains results would have predicted better conductivity for sample type C especially considering sample type T was performing better despite how little PANI was deposited. The PANI fibers appeared to be contributing to electrical percolation of the secondary phase whereas the montmorillonite was disrupting the conductive pathway. Accepting this analysis, the result is indicating that the pathways of PANI within the crazes, in almost all cases, only formed where a nucleating particle was present.

3.6. STRETCHABLE CONDUCTIVITY RESPONSE

Durability of the conductive network is an important property of flexible sensors, expanding the scope of their application. Through-plane and in-plane conductivity for the new, highly conductive P100 sample was monitored while undergoing deformation up to a strain of 15% to quantify the ability of the secondary phase to move without fracturing inside the

stretching polyethylene matrix. Fig. 9 presents both conductivity measurements and includes a tensile stress-strain curve obtained for P100 so that the elastoplastic response of the polymer can be related to the trend in conductivity. The in-plane conductivity, even undeformed, was more than three orders of magnitude lower than through-plane, indicating that the crazes forming the secondary phase network were mostly oriented transversely to the direction of elongation, likely due to the relatively small crystallites. The drop in in-plane conductivity occurred progressively while the polymer displayed an elastic response, reflecting brittle failures in the inter-connecting conductive pathways (i.e. branching pathways formed transversely to the direction of crazing). The near asymptotic decline in in-plane conductivity seen at 2-3% strain corresponded to yielding of the samples, after which the appearance of visible necking was seen.

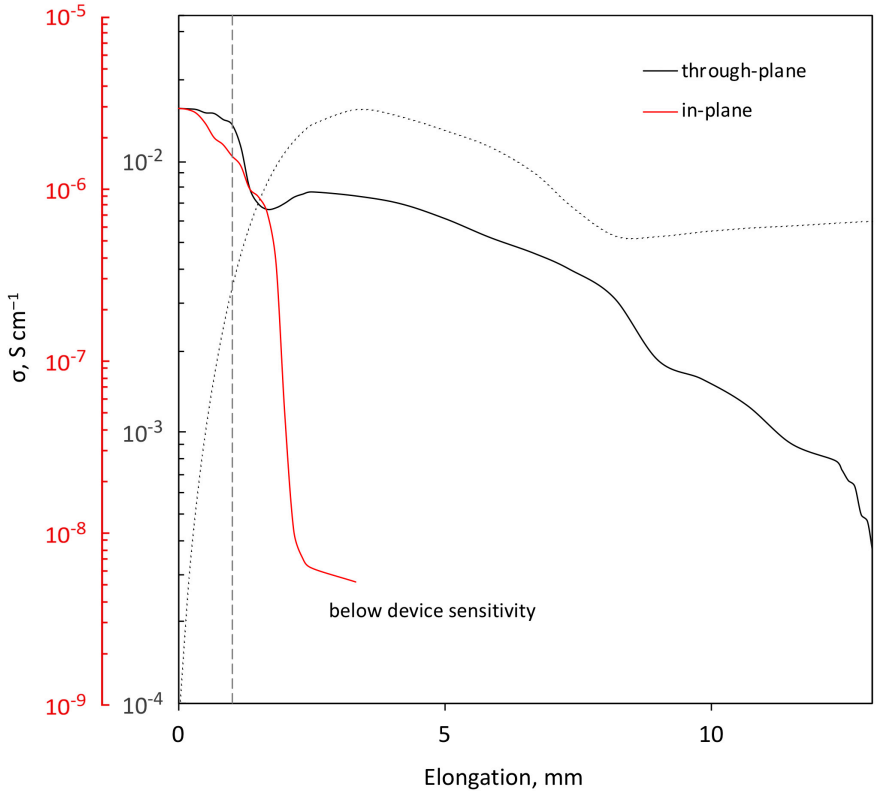

Figure 9. Through-plane and in-plane electrical conductivities change during deformation of P100 with an average tensile stress-strain curve. The dotted vertical line limits a stable range of about 1% strain within which the through-plane conductivity varies insignificantly.

The through-plane conductivity endured tensile deformation better, probably because the original crazing forming the secondary phase was largely transversely oriented and the tensile stresses therefore became concentrated at the polyethylene-PANI interface rather than in the PANI phase. At least while the polymer exhibited an elastic response, these transversely oriented PANI pathways were unaffected by the tensile deformation (less than 1% strain). Between 1% and 2% strain, through-plane conductivity decreased in a similar manner to in-plane conductivity. We believe the inter-connecting pathways (branches) were failing at the junction with the transversely oriented pathway, rather than in the middle of the branching pathway, causing a loss of conductivity in both the in-plane and through-plane direction for those pathways. Some plastic reorganization related to crystal slip was occurring in the sample structure,[34,35] though complete yielding had not yet occurred. Beyond the yielding point, further plastic deformation of the matrix polyethylene resulted in a slower yet gradual fragmentation of the conductive channels. However, even at 15% strain, the polymer remained quite conductive in the order of 10^{-3} $S \cdot cm^{-1}$.

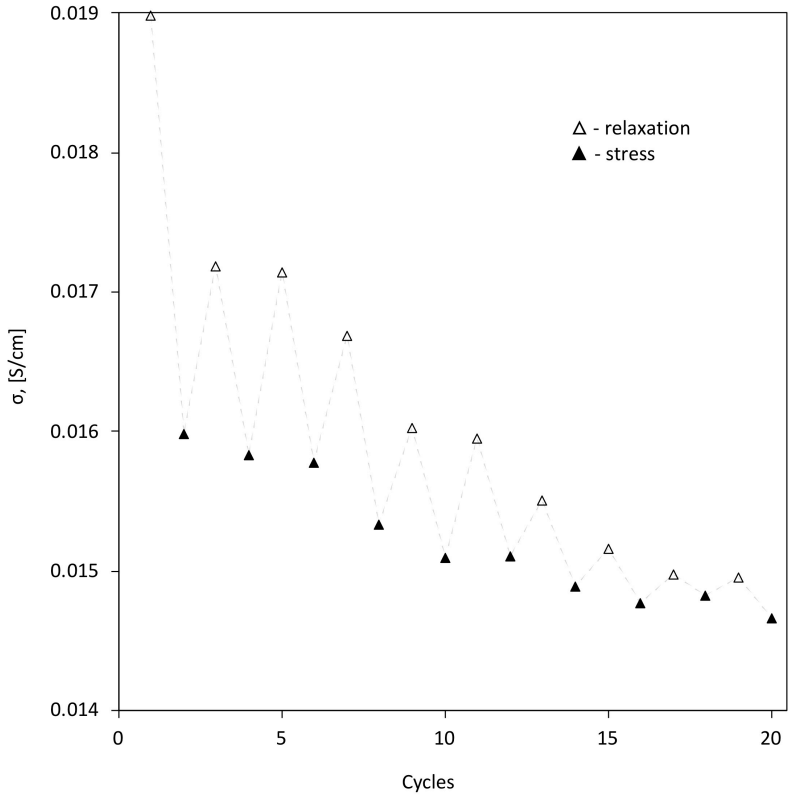

Figure 10. Cyclic deformation of P100 within the elastic limit of 1% strain for 10 cycles.

Cyclic deformation of P100 within the elastic limits (1% strain) showed a subtle irreversible change in conductivity per loading cycle, with a total decline of 5 $mS \cdot cm^{-1}$, after twenty cycles (Fig. 10). The difference in conductivity between the stress and relaxation stages decreased from cycle to cycle, reaching a value of 300 $\mu S \cdot cm^{-1}$ by the end of the test. Based on these results, cyclic deformation of the new conductivity polymer within 1% strain was considered adequately flexible in terms of both conductivity and elastic recovery.

4. CONCLUSION

The results in this paper expand on previous research for introducing advanced properties into otherwise inexpensive materials based on establishing controlled percolative pathways from intercrystalline crazing and polymerizing a secondary phase within those channels. In this regard, controlled crazing is associated with assist the penetration of a secondary phase monomer while retaining much of the physical nature of the matrix. Being inherently conductive, polyaniline was used to determine phase network continuity by measuring the in-plane and through-plane electrical properties of resulting samples. Different types of nucleating particles were examined in the study to vary the size of crystallites in the matrix prior to deformation. Montmorillonite and pre-synthesized PANI fibers produced similar size crystallites and correspondingly, crazes large enough for the ingress of the emulsified monomer, only the latter was effective in percolation. The compatibility of the PANI fibers with the polymerized in-situ polyaniline, formed a continuous, highly conductive network with overall composite conductivity of 2×10^{-2} $S\cdot cm^{-1}$, close in magnitude to pure doped polyaniline (1.2×10^{-1} $S\cdot cm^{-1}$). This sub-micron conductive network within polyethylene showed good retention of its electrical properties under cyclic stretching, indicating suitability for flexible electronics.

ACKNOWLEDGEMENT

The authors sincerely acknowledge the Natural Science and Engineering Research Council (NSERC) of Canada for supporting this fundamental research through Discovery Grant program. We also thank the Canada Foundation for Innovation (CFI) for the equipment and facilities. S.Z. thanks the Canada Research Chair (CRC) program for supporting his research.

REFERENCES

(1) J. Heeger, A. Polyaniline with Surfactant Counterions: Conducting Polymer Materials Which Are Processible in the Conducting Form. *Synth. Met.* **1993**, *57* (1), 3471–3482. https://doi.org/10.1016/0379-6779(93)90462-6.

(2) Osterholm, J.-E.; Cao, Y.; Klavetter, F.; Smith, P. Emulsion Polymerization of Aniline. *Polymer (Guildf).* **1994**, *35* (13), 2902–2906.

(3) Adams, P.; Laughlin, P.; Metals, A. M.-S.; 1996, undefined. Synthesis of High Molecular Weight Polyaniline at Low Temperatures. *Elsevier*.

(4) Kohlman, R. S.; Epstein, A. J. Insulator-Metal Transition and Inhomogeneous Metallic State in Conducting Polymers. *Handb. Conduct. Polym.* **1998**, *2*, 85–122.

(5) Ayad, M. M.; Salahuddin, N. A.; Alghaysh, M. O.; Issa, R. M. Phosphoric Acid and PH Sensors Based on Polyaniline Films. *Curr. Appl. Phys.* **2010**, *10* (1), 235–240. https://doi.org/10.1016/J.CAP.2009.05.030.

(6) Shabnam Virji, ‡; Richard B. Kaner, § and; Bruce H. Weiller*, ‡. Hydrogen Sensors Based on Conductivity Changes in Polyaniline Nanofibers†. **2006**. https://doi.org/10.1021/JP063166G.

(7) Kim, M.-S.; Kim, S.; Kong, H. J.; Kwon, O. S.; Yoon, H. Tunable Electrical-Sensing Performance of Random-Alternating Layered Graphene/Polyaniline Nanoarchitectures. *J. Phys. Chem. C* **2016**, *120* (32), 18289–18295. https://doi.org/10.1021/acs.jpcc.6b03705.

(8) Segal, E.; Tchoudakov, R.; Narkis, M.; Siegmann, A.; Yen Wei. Polystyrene/Polyaniline Nanoblends for Sensing of Aliphatic Alcohols. *Sensors Actuators B Chem.* **2005**, *104* (1), 140–150. https://doi.org/https://doi.org/10.1016/j.snb.2004.05.002.

(9) Kar, P.; Choudhury, A. Carboxylic Acid Functionalized Multi-Walled Carbon Nanotube Doped Polyaniline for Chloroform Sensors. *Sensors Actuators B Chem.* **2013**, *183*, 25–33. https://doi.org/10.1016/J.SNB.2013.03.093.

(10) Yang, C. Y.; Reghu, M.; Heeger, A. J.; Cao, Y. Thermal Stability of Polyaniline Networks in Conducting Polymer Blends. *Synth. Met.* **1996**, *79* (1), 27–32. https://doi.org/https://doi.org/10.1016/0379-6779(96)80126-3.

(11) Bhadra, S.; Khastgir, D.; Singha, N. K.; Lee, J. H. Progress in Preparation, Processing and Applications of Polyaniline. *Prog. Polym. Sci.* **2009**, *34* (8), 783–810. https://doi.org/https://doi.org/10.1016/j.progpolymsci.2009.04.003.

(12) Schilling, M.; Niebergall, U.; Alig, I.; Oehler, H.; Lellinger, D.; Meinel, D.; Böhning, M. Crack Propagation in PE-HD Induced by Environmental Stress Cracking (ESC) Analyzed by Several Imaging Techniques. *Polym. Test.* **2018**, *70*, 544–555. https://doi.org/https://doi.org/10.1016/j.polymertesting.2018.08.014.

(13) Saad, A. K.; Abdulhussain, H. A.; Gomes, F. P. C.; Vlachopoulos, J.; Thompson, M. R. Studying the Mechanism of Biodiesel Acting as an Environmental Stress Cracking Agent with Polyethylenes. *Polymer (Guildf).* **2020**, *191*, 122278. https://doi.org/https://doi.org/10.1016/j.polymer.2020.122278.

(14) Kornberg, A. B.; Thompson, M. R.; Zhu, S. Developing Continuous Submicron-Scale Conductive Interpenetrating Hydrogel Network in Polyethylene Matrices through Controlled Crazing and Polymerization. *Ind. Eng. Chem. Res.* **2020**, acs.iecr.9b07010. https://doi.org/10.1021/acs.iecr.9b07010.

(15) Volynskii, A. L.; Aleskerov, A. G.; Grokhovskaya, T. Y.; Bakeyev, N. F. Mechanical Behavior of Glassy Polyethylene Terephthalate Deformed in Liquid Adsorption Active

Media. *Polym. Sci. USSR* **1976**, *18* (9), 2419–2426.

(16) Volynskii, A. L.; Bakeev, N. F. *Solvent Crazing of Polymers*; Newnes, 2012; Vol. 13.

(17) Rozanski, A.; Galeski, A. Plastic Yielding of Semicrystalline Polymers Affected by Amorphous Phase. *Int. J. Plast.* **2013**, *41*, 14–29. https://doi.org/10.1016/J.IJPLAS.2012.07.008.

(18) Pawlak, A.; Galeski, A. Stability of Spherulite Growth Rate. *J. Polym. Sci. Part B Polym. Phys.* **1990**, *28* (10), 1813–1821. https://doi.org/10.1002/polb.1990.090281012.

(19) Nowacki, R.; Kolasinska, J.; Piorkowska, E. Cavitation during Isothermal Crystallization of Isotactic Polypropylene. *J. Appl. Polym. Sci.* **2001**, *79* (13), 2439–2448. https://doi.org/10.1002/1097-4628(20010328)79:13<2439::AID-APP1051>3.0.CO;2-#.

(20) Bucknall, C. B. New Criterion for Craze Initiation. *Polymer (Guildf).* **2007**, *48* (4), 1030–1041. https://doi.org/https://doi.org/10.1016/j.polymer.2006.12.033.

(21) Pawlak, A.; Galeski, A.; Rozanski, A. Cavitation during Deformation of Semicrystalline Polymers. *Prog. Polym. Sci.* **2014**, *39* (5), 921–958. https://doi.org/10.1016/J.PROGPOLYMSCI.2013.10.007.

(22) Han, Y.-G.; Kusunose, T.; Sekino, T. One-Step Reverse Micelle Polymerization of Organic Dispersible Polyaniline Nanoparticles. *Synth. Met.* **2009**, *159* (1–2), 123–131. https://doi.org/10.1016/J.SYNTHMET.2008.08.011.

(23) Stejskal, J.; Kratochvíl, P.; Jenkins, A. D. The Formation of Polyaniline and the Nature of Its Structures. *Polymer (Guildf).* **1996**, *37* (2), 367–369. https://doi.org/10.1016/0032-3861(96)81113-X.

(24) Federal Republic of Germany. Surface Tension Values of Some Common Polymers/Test Liquids for Surface Energy Analysis www.surface-tension.de.

(25) Gokel, G. W.; Dean, J. A. *Dean's Handbook of Organic Chemistry*; McGraw-Hill handbooks; McGraw-Hill, 2004.

(26) Rozanski, A.; Galeski, A. Controlling Cavitation of Semicrystalline Polymers during Tensile Drawing. *Macromolecules* **2011**, *44* (18), 7273–7287.

(27) Shreepathi, S.; Holze, R. Spectroelectrochemical Investigations of Soluble Polyaniline Synthesized via New Inverse Emulsion Pathway. *Chem. Mater.* **2005**, *17* (16), 4078–4085. https://doi.org/10.1021/cm050117s.

(28) Zheng, W.-Y.; Levon, K.; Taka, T.; Laakso, J.; Österholm, J.-E. Doping-Induced Layered Structure in N-Alkylated Polyanilines. *Polym. J.* **1996**, *28* (5), 412–418. https://doi.org/10.1295/polymj.28.412.

(29) Levon, K.; Ho, K.-H.; Zheng, W.-Y.; Laakso, J.; Kärnä, T.; Taka, T.; Österholm, J.-E. Thermal Doping of Polyaniline with Dodecylbenzene Sulfonic Acid without Auxiliary Solvents. *Polymer (Guildf).* **1995**, *36* (14), 2733–2738. https://doi.org/https://doi.org/10.1016/0032-3861(95)93650-B.

(30) Kumar, A.; Kumar, V.; Sain, P. K.; Kumar, M.; Awasthi, K. Synthesis and Characterization of Polyaniline Membranes with – Secondary Amine Additive Containing N,N′-Dimethyl Propylene Urea for Fuel Cell Application. *Int. J. Hydrogen Energy* **2018**, *43* (47), 21715–21723. https://doi.org/10.1016/J.IJHYDENE.2018.04.083.

(31) Zhang, F.; Halverson, P. A.; Lunt, B.; Linford, M. R. Wet Spinning of Pre-Doped Polyaniline into an Aqueous Solution of a Polyelectrolyte. *Synth. Met.* **2006**, *156* (14–15), 932–937. https://doi.org/10.1016/J.SYNTHMET.2006.06.002.

(32) Hassan, P. A.; Sawant, S. N.; Bagkar, N. C.; Yakhmi, J. V. Polyaniline Nanoparticles Prepared in Rodlike Micelles. *Langmuir* **2004**, *20* (12), 4874–4880.

https://doi.org/10.1021/la0498096.

(33) Tam, D. K. Y.; Ruan, S.; Gao, P.; Yu, T. 10 - High-Performance Ballistic Protection Using Polymer Nanocomposites. In *Woodhead Publishing Series in Textiles*; Sparks, E. B. T.-A. in M. T. and P. E., Ed.; Woodhead Publishing, 2012; pp 213–237. https://doi.org/https://doi.org/10.1533/9780857095572.2.213.

(34) Seguela, R.; Elkoun, S.; Gaucher-Miri, V. Plastic Deformation of Polyethylene and Ethylene Copolymers: Part II Heterogeneous Crystal Slip and Strain-Induced Phase Change. *J. Mater. Sci.* **1998**, *33* (7), 1801–1807. https://doi.org/10.1023/A:1004340902180.

(35) Gomes, F. P. C.; West, W. T. J.; Thompson, M. R. Effects of Annealing and Swelling to Initial Plastic Deformation of Polyethylene Probed by Nonlinear Ultrasonic Guided Waves. *Polymer (Guildf).* **2017**, *131*, 160–168. https://doi.org/https://doi.org/10.1016/j.polymer.2017.10.041.